ACS APPLIED MATERIALS & INTERFACES

Research Article

www.acsami.org

# Rational Design of High-Surface-Area Carbon Nanotube/Microporous Carbon Core–Shell Nanocomposites for Supercapacitor Electrodes

Yuanyuan Yao,[†] Cheng Ma,[†] Jitong Wang,[†] Wenming Qiao,[†] Licheng Ling,[†,‡] and Donghui Long*[,†,‡]

[†]State Key Laboratory of Chemical Engineering and [‡]Key Laboratory of Specially Functional Polymeric Materials and Related Technology, East China University of Science and Technology, Shanghai 200237, China

Supporting Information

**ABSTRACT:** All-carbon-based carbon nanotube (CNT)/microporous carbon core–shell nanocomposites, in which a CNT as the core and high-surface-area microporous carbon as the shell, have been prepared by in situ resorcinol–formaldehyde resin coating of CNTs, followed by carbonization and controlled KOH activation. The obtained nanocomposites have very high Brunauer–Emmett–Teller surface areas (up to 1700 $m^2/g$), narrow pore size distribution (<2 nm), and 1D tubular structure within a 3D entangled network. The thickness of the microporous carbon shell can be easily tuned from 20 to 215 nm by changing the carbon precursor/CNT mass ratio. In such a unique core–shell structure, the CNT core could mitigate the key issue related to the low electronic conductivity of microporous carbons. On the other hand, the 1D tubular structure with a short pore-pathway micropore as well as a 3D entangled network could increase the utilization degree of the overall porosity and improve the electrode kinetics. Thus, these CNT/microporous carbon core–shell nanocomposites exhibit a great potential as an electrode material for supercapacitors, which could deliver high specific capacitance of 237 F/g, excellent rate performance with 75% maintenance from 0.1 to 50 A/g, and high cyclability in $H_2SO_4$ electrolyte. Moreover, the precisely controlled microporous carbon shells may allow them to serve as excellent model systems for microporous carbons, in general, to illustrate the role of the pore length on the diffusion and kinetics inside the micropores.

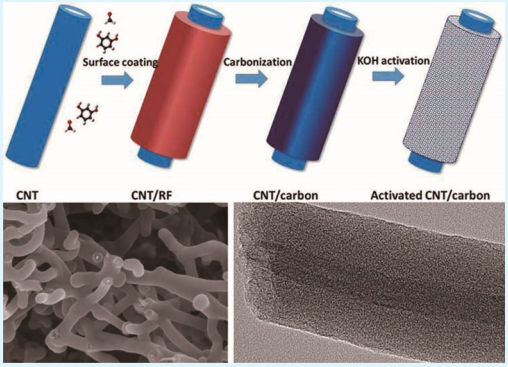


**KEYWORDS:** *microporous carbon, carbon nanotube, core–shell structure, supercapacitor, frequency response*

## INTRODUCTION

Supercapacitors have attracted considerable attention with their series of unique advantages (high specific power, fast charge and discharge processes, long cycle life, etc.).[1−3] Porous carbon materials such as activated carbons are the most commonly used materials as electrodes in supercapacitor devices, as carbon materials can have high surface area, are chemically and thermally stable, of relatively low cost, and are environmentally friendly.[4−9] When carbon materials are employed as electrode materials, the following characteristics are commonly required: (1) high specific surface area to accumulate and keep the charges on the thin layer of the electrode/electrolyte interface; (2) suitable pore size distribution and pore length for facilitating the diffusion of ions; (3) outstanding electrical conductivity for efficient conductive networks; (4) robust mechanical and electrical stability to maintain the long-term cycling performance of electrodes.[10−12] Although very high surface area can be easily achieved for activated carbons prepared by KOH activation, their relatively poor electrical conductivity,[13] originating from the short-range $sp^2$ bonding and a large amount of structural defects,[14] may limit the power characteristics of supercapacitors. In addition, the predominant endohedral surface of the microporous structure results in the transfer limitation of electrolyte ions during rapid charge and discharge processes, deteriorating its rate capability.[15−17] Thus, various approaches including improving the carbon conductivity,[18] constructing a hierarchical pore system,[19] adding mesoporosity,[20] and reducing the dimensions of carbon particles to the nanoscale[14] have been widely used by researchers.

Carbon nanotubes (CNTs) have excellent electrical conductivity, high mechanical strength, and chemical stability.[21−23] However, CNTs with closed tips have only limited accessible surface area (typically less than 200 $m^2/g$), which restricts the direct usage of CNTs as electrodes for supercapacitors.[24] An enhancement of the specific capacitance given by CNTs could be achieved by mixing with pseudocapacitive active materials to introduce the fast redox reactions. Various active materials, like conductive polymers polypyrrole,[25,26] PANI,[27] or metal oxide $RuO_2$,[28] $MnO_2$,[29,30] or $NiCo_2O_4$,[31] have been directly grown on

Received: December 11, 2014
Accepted: February 5, 2015
Published: February 5, 2015





DOI: 10.1021/am5087374
ACS Appl. Mater. Interfaces 2015, 7, 4817−4825

the external surface of CNTs. These hybrid structures could achieve both high conductive performance and high surface area/volume ratio as an electrode for supercapacitors.

A rational combination of CNTs and porous carbons could also improve the capacitive performance based on the pure principle of an electrochemical double layer. The embedding of CNTs in the porous carbon matrix could help create networks with better electrical conductivity and mechanical stability, thus demonstrating highly stable capacitive performance at a high rate. Various integrated CNT/porous carbon composites including CNT/activated carbon,[32−34] CNT/biopolymer-based carbon,[20] CNT/N-doped carbon,[35] and phosphate-functionalized CNT/carbon[36] have been fabricated via carbonization and/or activation of CNT/polymer composites. However, in these mentioned reports, the CNTs were mostly dispersed randomly in the carbon matrices, which might be flocculated into bundles or agglomerates because of strong van der Waals interactions during mixing and casting procedures. Until now, there are only limited reports on the development of well-designed CNT/carbon composites, especially for the unique core−shell tubular structure. This is possibly due to the poor CNT dispersion in solution or weak interaction of a guest polymer with the CNT surface.[37−39] Recently, Qian et al.[40] made a first attempt to prepare multiwalled carbon nanotube@mesoporous carbon composites by combining a coating pathway and a nanocasting strategy. The obtained composite materials showed a unique tubular core−shell structure but with a relatively low Brunauer−Emmett−Teller (BET) surface area of 606 $m^2/g$. In addition, the synthesis needed the tedious steps that might limit their wide applications as electrode materials. Therefore, there is still a challenge of the direct configuration of high-surface-area CNT/carbon core−shell nanocomposites by a facile method.

Herein, we developed a facile method to prepare high-surface-area CNT/microporous carbon composite materials for supercapacitor electrodes. The individual nanotube was uniformly coated with resins by in situ chemical polymerization of resorcinol−formaldehyde, followed by carbonization and controlled KOH activation. The obtained nanocomposites have a unique core−shell heterostructure with a CNT as the core and high-surface-area microporous carbon as the shell, which is distinct from conventional CNT-modified porous carbons that were composed of a micron-sized or larger skeleton. In such a core−shell nanostructure, the CNT core may mitigate the key issue related to the low electronic conductivity of microporous carbons. On the other hand, by creating a microporous carbon shell with a short diffusion path and high microporosity, instead of larger pores (little contribution to capacitance), these nanocomposites could greatly increase the utilization degree of the overall porosity and surface area. Therefore, these well-tailored core−shell nanostructures with a synergistic combination of short diffusion path, high microporosity, and good electrical conductivity should have great potential as electrode materials for supercapacitor applications. In addition, the final core−shell structure of the composite can be easily tailored, which is crucial for illustrating the role of a conductive network as well as short-pore-length pores and understanding the frequency response and dynamic changes on the electrode.

## EXPERIMENTAL SECTION

**Material Preparation.** An aqueous dispersion of CNTs (TNWDM, 8 wt %) was purchased from Chengdu Organic Chemicals Co. Ltd. without further treatment. The CNT/amorphous carbon composites were prepared by in situ chemical coating of resorcinol−formaldehyde resin onto CNTs, followed by carbonization and activation. In the synthesis procedure, 6.46 g of resorcinol and 9.54 g of formaldehyde (37 wt % solution) were added into 200 mL of deionized water under constant stirring until resorcinol was dissolved. Then a certain amount of the aqueous dispersion of CNTs was added into the solution under ultrasound treatment for 10 min. The mixture was then stirred at 80 °C for a certain time (8−24 h). The obtained polymer-coated CNTs were separated and dried at 100 °C. The yield of polymer is around 90% for each batch. In this work, the amount of CNT dispersion used was changed to adjust the shell thickness of the composites. The obtained RF polymer-coated CNTs are denoted as CNT/RF-*x*, where *x* is represented of the mass ratio of RF to CNTs. The CNT/RF-*x* nanocomposites were carbonized at 800 °C in $N_2$ flow for 3 h at the rate of 5 °C/min to obtain the CNT/carbon-*x* composites.

The $CO_2$ activation was performed by placing a ceramic boat with 1 g of CNT/carbon-*x* composites in a tube furnace under flowing nitrogen with a heating rate of 5 °C/min up to 900 °C. After this temperature was reached, the activating gas was introduced for 2 h and then switched back to nitrogen to prevent further activation during the cooling process. Activation of all samples was performed at 900 °C for 2 h. The $CO_2$-activated samples are denoted as CA-CNT/carbon-*x*, where *x* designates the weight ratio of RF polymer to CNTs.

The KOH activation was performed by placing a nickel boat with 3 g of KOH and 1 g of the CNT/carbon-*x* under a $N_2$ flow at 800 °C for 2 h. The obtained materials were liberated by removing inorganic salts using 2 mol/L HCl and washed with deionized water until a neutral pH. The prepared CNT/activated carbon composites are denoted as KA-CNT/carbon-*x*, where *x* designates the weight ratio of RF polymer to CNTs.

**Characterization.** The weight contents of the CNT in the composites are calculated based on the presumption that the CNTs were fully retained in the polymer composites after the filtering and did not experience the weight loss during carbonization and activation processes. The morphologies of the nanocomposites were observed under scanning electron microscopy (SEM, JEOL 7100F). The microstructures were observed under transmission electron microscopy (TEM, JEOL 2100F) operated at 200 kV. Nitrogen adsorption/desorption isotherms were measured at 77 K with a Quadrasorb SI analyzer. Before the measurements, the samples were degassed in vacuum at 473 K for 12 h. The BET method was utilized to calculate the specific surface areas ($S_{BET}$). The pore size distributions were determined from the quenched solid-state density functional theory (DFT) model. The total pore volumes ($V_{total}$) were estimated from the amount adsorbed at the maximal relative pressure of 0.985. Micropore surface areas ($S_{micro}$) and pore volume ($V_{micro}$) were obtained via the DFT method. The X-ray diffraction (XRD) patterns were acquired on a Rigaku D/max 2550 diffractometer operating at 40 kV and 20 mA using Cu K$\alpha$ radiation ($\lambda$ = 1.5406 Å).

**Electrochemical Test.** The KA-CNT/carbon-*x* powders were processed into capacitor electrodes by mixing them with poly(tetrafluoroethylene) (5 wt %) and acetylene black (5 wt %) homogenized in a mortar and pestle, then rolled into a thin film of uniform thickness, and finally punched into pellets. Each electrode contained active materials of ∼10 mg and had a thickness of ∼80 $\mu$m and a geometric diameter of about 1 cm. The packing density of each sample is around 0.16 $g/cm^3$. Electrochemical experiments were carried out with Teflon Swagelok-type two-electrode configuration, which was constructed with two facing carbon electrodes, sandwiched with a separator. $H_2SO_4$ (3 M) was employed as the electrolyte.

The electrochemical behaviors of the KA-CNT/carbon-*x* materials were measured by cyclic voltammetry (CV) and electrochemical impedance spectroscopy (EIS) analysis (Gamry Instrument, Warminster, PA, USA). CV was performed in the voltage range of 0−0.9 V and EIS with the frequency in the range from 1 mHz to 100 kHz, ac amplitude, 5 mV. Galvanostatic charge−discharge tests were conducted to estimate the specific capacitance of samples on a RABIN BT2000 apparatus. The gravimetric capacitance of the electrode material was calculated according to the equation $C$ =


DOI: 10.1021/am5087374
ACS Appl. Mater. Interfaces 2015, 7, 4817−4825

$2I\Delta t/(\Delta Vm)$, where $I$ is the discharge current, $\Delta t$ is the discharge time from 0.9 to 0 V, $\Delta V$ is the working voltage, and $m$ is the mass of carbon on an electrode.

## RESULTS AND DISCUSSION

**Preparation of the CNT/Carbon Nanocomposites.** The fabrication of the CNT/microporous carbon core−shell nanocomposites is illustrated in Figure 1. Keys to the success

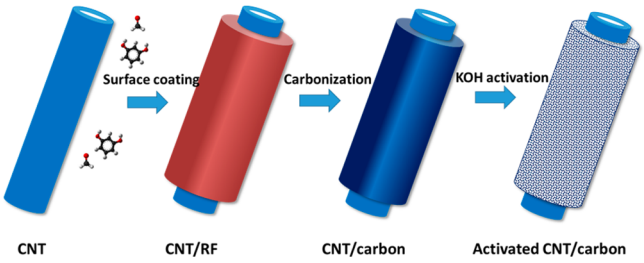


**Figure 1.** Illustration of the preparation of the CNT/microporous carbon core−shell nanocomposites.

of our synthesis approach lie in the uniform coating of resorcinol−formaldehyde polymer onto the surface of CNTs that can preserve the core−shell structure during pyrolysis and activation processes. The CNT dispersions with 8 wt % concentration were obtained from the commercial source and used instead of the CNT powders to solve the difficult dispersion of CNTs, which have a nonionic surfactant for superior dispersion and stability. After being mixed, the RF oligomer with plenty of hydrophilic groups would be preferably adsorbed on the surface of CNTs with the nonionic surfactant. With prolonged reaction time, the thickness of the RF shell gradually increases (Supporting Information Figure S1), suggesting the layer-by-layer coating process. In addition, by turning the initial mass ratio of RF/CNT, the thickness of the RF shell could be easily adjusted. Thus, after carbonization and activation, the CNT/carbon core−shell nanocomposites with controlled thickness of the amorphous carbon shell could be obtained. The CNT contents in the polymer composites can be calculated to be 18.6, 10.1, 4.4, and 2.3%, according to the yields and thermogravimetric (TG) analysis in Figure S2.

The direct carbonization of the CNT/RF polymer nanocomposites could result in the formation of the CNT/carbon core−shell nanocomposites. Figure 2 shows the SEM images of the pristine CNTs (Figure 2a) and the CNT/carbon core−shell nanocomposites. Compared with the pristine CNTs, the nanocomposites preserve well the one-dimensional tubular structure of the CNTs but with apparently thickened diameter (Figure 2b−e). The average outer diameter of the pristine CNTs is about 50 nm, and after being coated with carbon, the average diameter increases to about 90, 140, 300, and 480 nm, respectively. Because the yield of the RF polymer is almost the same at ∼90% for each sample, the diameter of the obtained composites is strongly dependent on the initial mass ratio of RF/CNT. By further fitting the diameter versus mass ratio of RF/CNT, we established a linear relationship between the two variables, showing a high correlation coefficient of 0.995 (Figure 2f). This enables one to alter the amorphous carbon shell thickness continuously over a wide range of 20−215 nm by changing the mass ratio of the reactants. The CNT/carbon core−shell nanocomposites still have a very smooth surface, indicating the compact and uniform coating of the carbon. The TEM images in Figure 3 also confirm that the amorphous

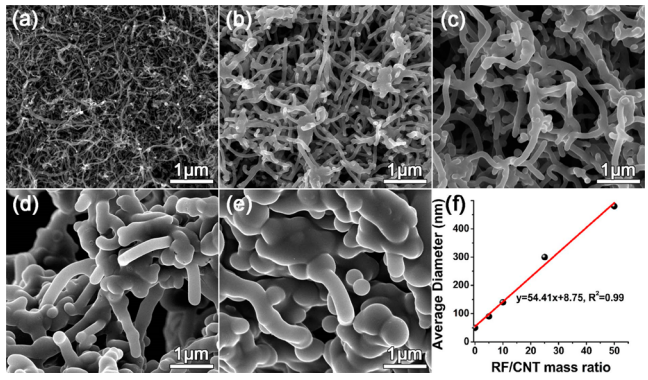


**Figure 2.** SEM images of the pristine CNTs (a), CNT/carbon-5 (b), CNT/carbon-10 (c), CNT/carbon-25 (d), and CNT/carbon-50 (e) nanocomposites (e), and the relationship between the RF/CNT mass ratio and the average diameter of the CNT/carbon nanocomposites (f).

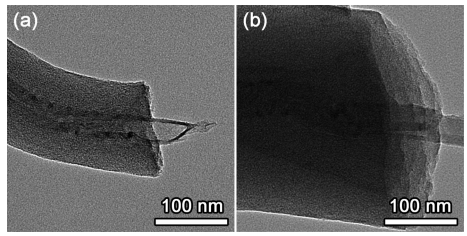


**Figure 3.** TEM images of the CNT/carbon core−shell nanocomposites: CNT/carbon-10 (a) and CNT/carbon-25 (b).

carbon shells with different thickness could be continuously wrapped on the sidewall of CNTs. These results clearly demonstrate the strong shape and structure-directing role of CNTs during the formation processes. If we assume that the CNTs do not experience weigh loss during carbonization, the CNT content is estimated to be about 30.6, 22.6, 11.1, and 6.5 wt % in the carbonized composites for CNT/carbon-5, CNT/carbon-10, CNT/carbon-25, and CNT/carbon-50, respectively.

During the carbonization, the RF polymer shell could be converted into the amorphous carbon shell as revealed by TEM observation (Figure 3) and XRD patterns (Figure S3). Meanwhile, considerable microporous structure could be created by the decomposition and release of small organic molecules during carbonization. Figure 4 shows $N_2$ adsorption−desorption isotherms and the resulting DFT pore size distributions of the pristine CNTs and the CNT/carbon core−shell nanocomposites. The pristine CNTs have a type III adsorption isotherm with an H3 hysteresis loop in IUPAC classification, indicating the slit-shaped mesopores raised from the packing of CNT aggregates. In contrast, the curves for all the CNT/carbon core−shell samples exhibit type I with a sharp increment at low relative pressure, which indicates the presence of considerable micropores. The DFT pore size distributions (Figure 4b) show that the CNT/carbon core−shell nanocomposites have relatively narrow micropore size distribution centered at 0.6−0.7 nm. The detailed porosity parameters are summarized in Table 1. With the mass ratio of RF/CNT increasing, the specific surface area gradually increases up to 818 $m^2/g$. The thicker the amorphous carbon shell, the higher the specific surface area achieved for the nanocomposites.

**Preparation of the $CO_2$-Activated CA-CNT/Carbon Composites.** Although direct carbonization of CNT/RF


DOI: 10.1021/am5087374
ACS Appl. Mater. Interfaces 2015, 7, 4817−4825

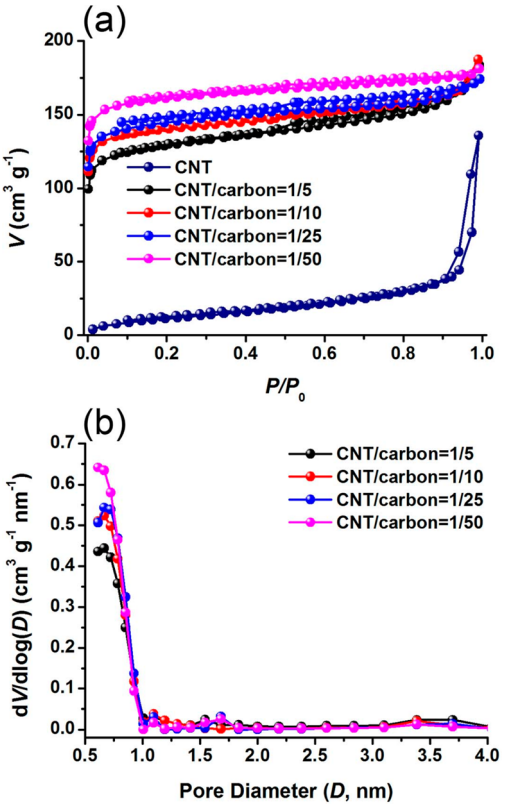


**Figure 4.** $N_2$ adsorption−desorption isotherms (a) and DFT pore size distributions (b) of the pristine CNTs and the CNT/carbon nanocomposites.

**Table 1. Porosity Parameters and CNT Content of the Pristine CNT and CNT/Carbon Nanocomposites**

| sample | CNT content (%) | $S_{BET}$[a] ($m^2/g$) | $S_{micro}$[b] ($m^2/g$) | $V_{total}$[c] ($cm^3/g$) | $V_{micro}$[d] ($cm^3/g$) |
|---|---|---|---|---|---|
| pristine CNTs | 98[e] | 44 | | 0.21 | |
| CNT/carbon-5 | 30.6 | 498 | 418 | 0.3 | 0.17 |
| CNT/carbon-10 | 22.6 | 549 | 493 | 0.32 | 0.2 |
| CNT/carbon-25 | 11.1 | 609 | 563 | 0.31 | 0.24 |
| CNT/carbon-50 | 6.5 | 818 | 757 | 0.34 | 0.28 |
| CA-CNT/carbon-5 | | 998 | 739 | 0.99 | 0.3 |
| CA-CNT/carbon-10 | | 1059 | 886 | 0.82 | 0.35 |
| CA-CNT/carbon-25 | | 1042 | 933 | 0.65 | 0.37 |
| CA-CNT/carbon-50 | | 1014 | 941 | 0.56 | 0.37 |
| KA-CNT/carbon-5 | 43.7 | 1020 | 762 | 0.45 | 0.38 |
| KA-CNT/carbon-10 | 33.2 | 1240 | 1109 | 0.79 | 0.47 |
| KA-CNT/carbon-25 | 16.6 | 1598 | 1458 | 0.81 | 0.61 |
| KA-CNT/carbon-50 | 10.1 | 1705 | 1582 | 0.82 | 0.75 |

[a]BET specific surface area. [b]Micropore (<2 nm) surface area calculated by DFT method. [c]Total pore volume at $P/P_0$ = 0.995. [d]Micropore (<2 nm) volume calculated by DFT method. [e]Determined from TG results.

polymer nanocomposites could produce the CNT/carbon nanocomposites with a certain amount of micropores, higher surface area is generally necessary for carbon materials in adsorption and electrochemical applications where the micropore plays a dominate role.[41] In order to increase the microporosity, the carbonized materials were further activated by using $CO_2$ as the gasifying agent or using KOH as the chemical-activating agent.

$CO_2$ is a mild oxidant at 800−950 °C, which can eliminate carbon atoms via the reaction $C + CO_2 \leftrightarrow 2CO$, in such a way as to favor the selective burning of the interior of the carbon materials with the subsequent creation of porosity.[42] In the present work, the CNT/carbon nanocomposites were activated by $CO_2$ at 900 °C for 2 h. The $N_2$ adsorption−desorption isotherms and resulting DFT microporous size distributions of the $CO_2$-activated CA-CNT/carbon nanocomposites are shown in Figure 5. An initial rapid increase in the nitrogen

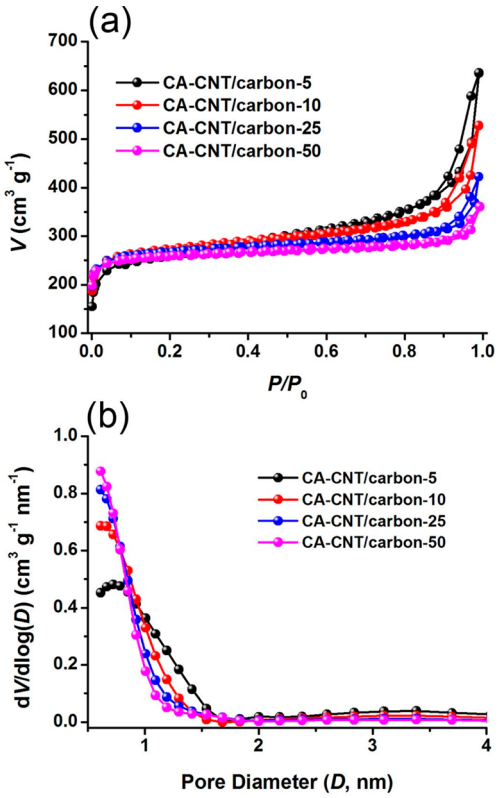


**Figure 5.** $N_2$ adsorption−desorption isotherms (a) and the resulting DFT pore size distributions (b) of the $CO_2$-activated CA-CNT/carbon nanocomposites.

adsorbed is observed below $P/P_0$ = 0.05, indicating the presence of abundant micropores. The DFT pore size distributions reveal that the $CO_2$-activated samples still have relatively narrow micropores with the average pore size <1 nm. In addition, the appearance of hysteresis at high $P/P_0$ suggests that $CO_2$ activation may produce some mesopores. As can be seen from Table 1, the surface area of the $CO_2$-activated CA-CNT/carbon nanocomposites is around 1000 $m^2/g$, which indicates an approximate 200−500 $m^2/g$ enhancement compared to the respective non-activated samples.

Generally, $CO_2$ activation is a mild process which does not destroy the structural morphology of the carbons as much.[43,44] However, SEM images (Figure 6a,b) reveal that the CNT/carbon-5 and CNT/carbon-10 experience severe corrosion and destruction after $CO_2$ activation. Some tubular structures are cut down into small fragments and are damaged, creating many cavities. From TEM observations (Figure 6c,d), it is found that some $CO_2$-activated samples possess larger hollow cores, indicating that $CO_2$ can react with the inner CNTs and damage the CNTs. Similarly, Chen et al. also observed that MWNTs activated by $CO_2$ possessed larger hollow tubes.[45] It is


DOI: 10.1021/am5087374
ACS Appl. Mater. Interfaces 2015, 7, 4817−4825

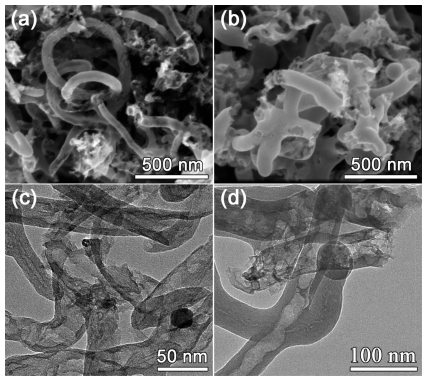


**Figure 6.** SEM images of the $CO_2$-activated CA-CNT/carbon nanocomposites: CA-CNT/carbon-5 (a), CA-CNT/carbon-10 (b); TEM images of CA-CNT/carbon-5 (c) and CA-CNT/carbon-10 (d).

well-accepted that $CO_2$ preferentially reacts with the amorphous carbons rather than graphitic carbons.[46] Thus, one possible reason for the larger hollow cores is due to the residual catalyst Fe nanoparticles that are trapped in the CNTs (~2% from TG results in Figure S4), which promote the catalytic gasification.[47]

**Preparation of the KOH-Activated KA-CNT/Carbon Nanocomposites.** It is necessary to develop an appropriate activation method to introduce more micropores into amorphous carbon shells while maintaining the shapes and properties of the CNT cores. Here we are able to demonstrate that the KOH activation could achieve this goal. The reaction of carbon and KOH starts with solid–solid reactions and then proceeds via solid–liquid reactions.[48] Due to the 3D open entangled network and predeveloped microporous structure of the CNT/carbon nanocomposites, KOH could be easily infiltrated into the carbon structure for homogeneous dispersion and activation.

As shown in Figure 7, SEM images of the KOH-activated KA-CNT/carbon nanocomposites show a uniform 1D tubular

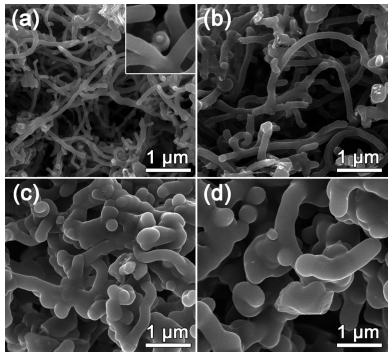


**Figure 7.** SEM images of the KOH-activated KA-CNT/carbon core–shell nanocomposites: KA-CNT/carbon-5 (a), KA-CNT/carbon-10 (b), KA-CNT/carbon-25 (c), and CNT/carbon-50 (d).

structure without separated segments, and the surface seems similarly smooth as those of the unactivated samples. The average diameters of the KOH-activated samples are about 85, 130, 280, and 460 nm respectively, slightly smaller than those of their unactivated counterparts. The TEM images (Figure 8) demonstrate that the developed microporous carbon shells with different thicknesses could be uniformly wrapped around the CNTs. The KOH should react with the carbon from outside to

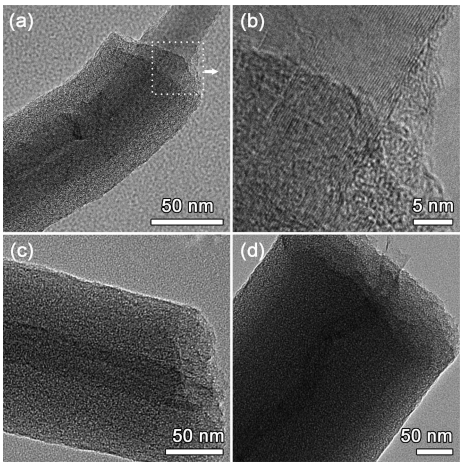


**Figure 8.** TEM images of the KOH–CNT/activated carbon nanocomposites: KA-CNT/carbon-5 (a) and magnification of KA-CNT/carbon-5 (b), KA-CNT/carbon-10 (c), KA-CNT/carbon-25 (d).

inside, thus suppressing the etching of the CNTs. Such outside-to-inside reaction of the CNT/carbon nanocomposites with KOH endows the nanocomposites with electron pathways and short-pore-length microporous shell, which may play a critical role in enhancing the electrode kinetics of their electrochemical applications.

Figure 9 shows the $N_2$ adsorption–desorption isotherms and resulting DFT pore size distributions of the KOH-activated samples. With the same activation conditions, the nano-

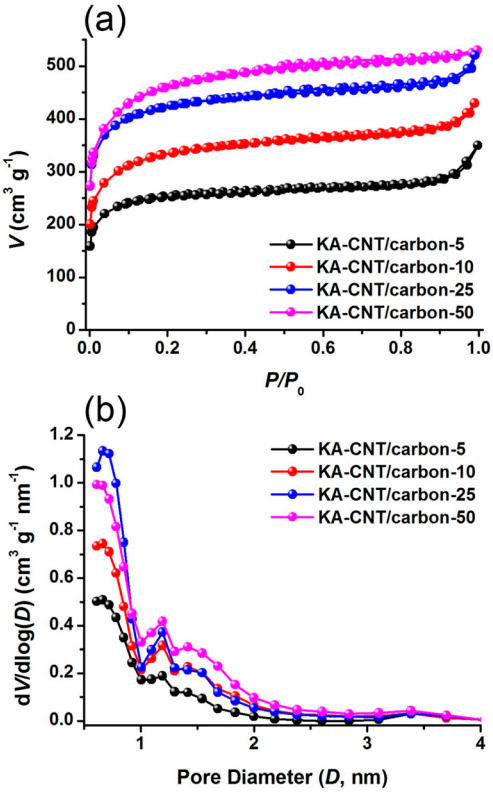


**Figure 9.** $N_2$ adsorption–desorption isotherms (a) and DFT pore size distributions (b) of the KOH-activated KA-CNT/carbon nanocomposites.


DOI: 10.1021/am5087374
ACS Appl. Mater. Interfaces 2015, 7, 4817–4825

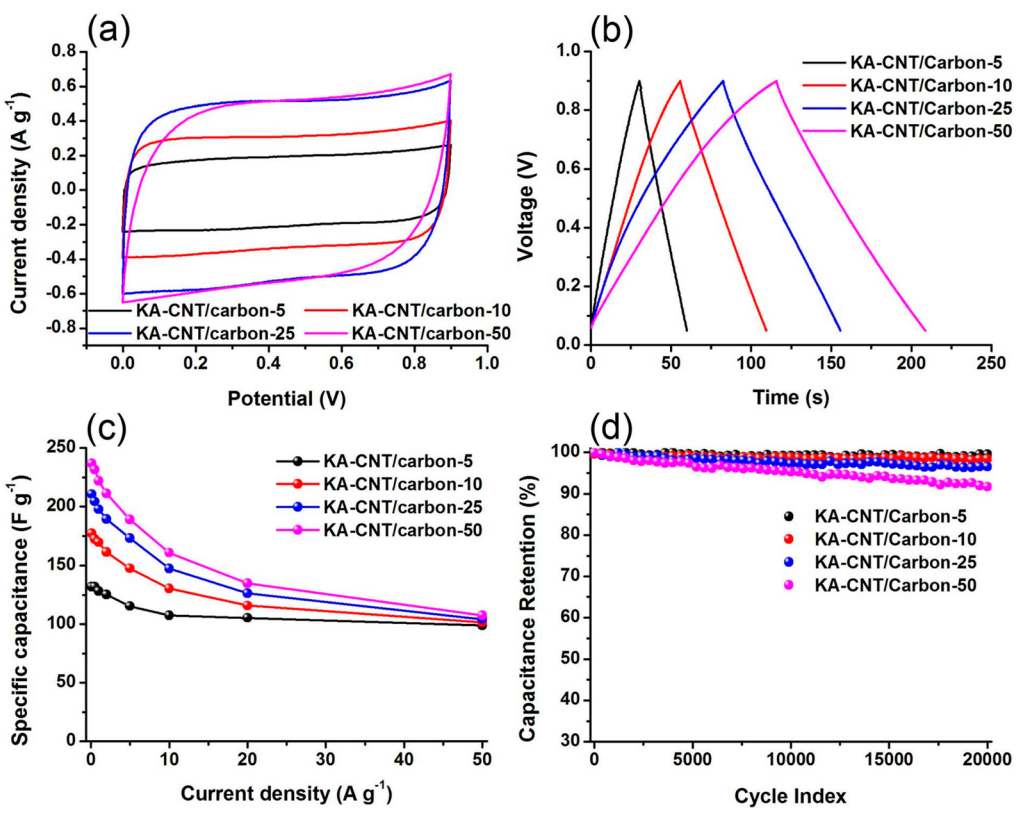


**Figure 10.** Electrochemical performance of the KOH-activated KA-CNT/carbon nanocomposites: (a) CV curves at 20 mV/s, (b) galvanostatic charge/discharge curves at 1 A/g, (c) rate performances, and (d) cycling performances.

composites with thicker shells have obviously higher porosity, due to the CNT cores contributing a little to the total porosity. From Figure 9b, the KOH-activated samples have pore size predominantly ranging from 0.7 to 2 nm, significantly wider than those of unactivated and $CO_2$-activated samples. In addition, the surface areas of the KOH-activated nanocomposites significantly increase to 1020−1705 $m^2/g$, almost double that of the unactivated counterparts. If we further assume that the CNTs experience no weight loss during KOH activation, the content of CNTs in the KA-CNT/carbon-5, KA-CNT/carbon-10, KA-CNT/carbon-25, and KA-CNT/carbon-50 can be estimated as 43.7, 33.2, 16.6, and 10.1 wt %, respectively. By subtracting the contribution of the CNT core to the total surface area, the microporous carbon shells for all samples have almost similar specific surface areas of ~1900 $m^2/g$ with the same pore size distribution. Thus, these unique CNT/carbon core−shell nanocomposites with a controllable microporous carbon shell will allow them to serve as excellent model systems for illustrating the role of pore length on diffusion and other general performance of microporous carbons.

**Electrochemical Performance of the KOH-Activated KA-CNT/Carbon Nanocomposites.** To test the performance of these high-surface-area KA-CNT/carbon core−shell nanocomposites, symmetrical cells with a two-electrode configuration were constructed to simulate actual device behavior. The CV testing (Figure 10a) shows very rectangular curves from 0 to 0.9 V at a scan rate of 20 mV/s, confirming the formation of an efficient electric double layer and fast charge propagations within the electrodes. Even at a scan rate of 100 mV/s, the CV curves of the samples still remain quasi-rectangular with only little variance, indicating high rate performance for supercapacitors (Figure S5). The galvanostatic charge/discharge curves at a current density of 1 A/g are shown in Figure 10b. The voltage drops at the initiation of the discharge are negligible for all samples. The specific capacitances are calculated from the discharge curves with values of 131.8, 177.3, 210.7, and 237.0 F/g for KA-CNT/carbon-5, KA-CNT/carbon-10, KA-CNT/carbon-25, and KA-CNT/carbon-50, respectively, in proportion with the specific surface area of the nanocomposites. If we neglect the capacitive contribution of the CNT cores, the microporous carbon shells for all samples can deliver the similar capacitance of around 13 $\mu F/cm^2$. This is in agreement with the reported range of 7−21 $\mu F/cm^2$ for carbon materials.[49−51]

To evaluate the rate capability of all samples, the capacitance and its retention ratio versus the charge/discharge current density are plotted in Figure 10c and Figure S6. In general, the supercapacitor performance of these materials does not show much degradation with an increase in the current density. However, the nanocomposites with a thinner microporous carbon shell show obviously superior rate performances. As the current density increases from 0.1 to 50 A/g, the capacitance of KA-CNT/carbon-5 decreases only 24.9% while that of KA-CNT/carbon-50 decreases 55.3%. Apparently, this rate performance difference should be ascribed to the ion diffusion path and the conductivity of the electrode materials. Furthermore, cycling performance of the KA-CNT/carbon-5, KA-CNT/carbon-10, KA-CNT/carbon-25, and KA-CNT/carbon-50 electrodes shows that nearly 99, 98, 96, and 92% of their initial capacitances (1 A/g) are maintained after 20 000 cycles (Figure 10d), indicating excellent physical stabilities and apparent cyclabilities for the electrodes. In addition, there is a general tendency that the capacitance retention slightly


DOI: 10.1021/am5087374
ACS Appl. Mater. Interfaces 2015, 7, 4817−4825

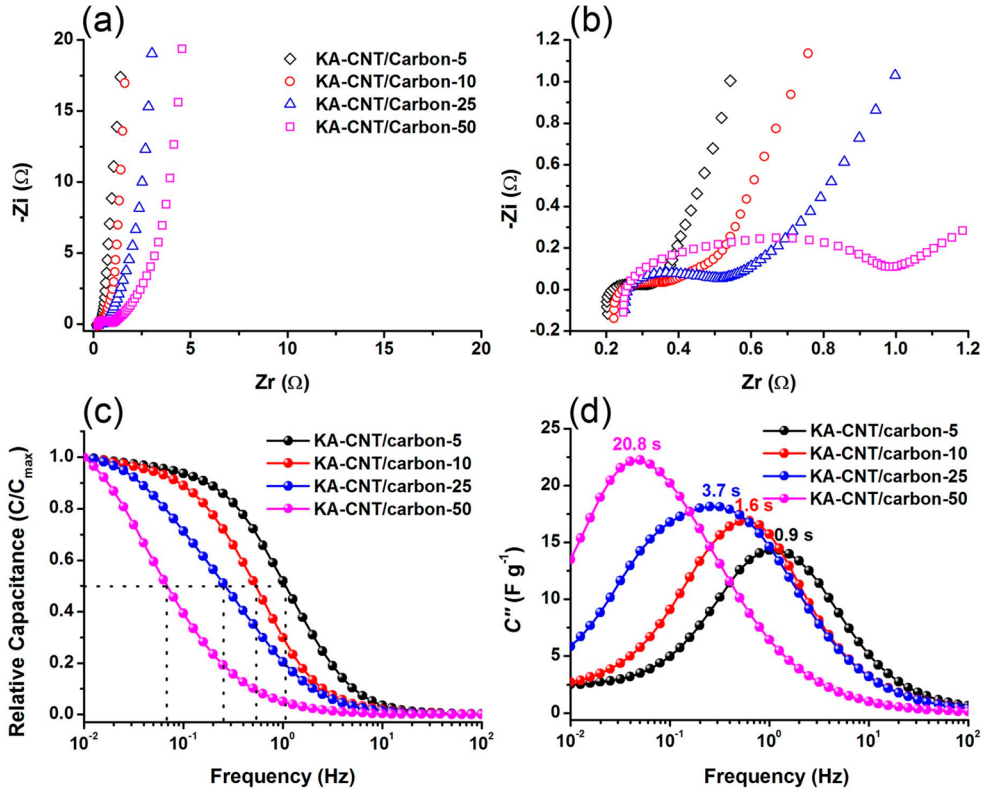


**Figure 11.** Nyquist plots (a) and the enlargement of the high-frequency region (b), evolution of the relative real capacitance (c), and imaginary capacitance (d) with frequency for the KOH-activated KA-CNT/carbon nanocomposites.

decreases with the thickness of activated carbon shell increasing.

To reveal the charge−discharge kinetics inside these KA-CNT/carbon core−shell nanocomposites with different thicknesses, the EIS testing was performed, as illustrated in Figure 11. Each Nyquist plot is composed of a semicircle at high frequency and a nearly vertical line at low frequency. The vertical line indicates the ideal capacitive behavior of the cell. The intercept of the curve with the real impedance axis represents the internal or equivalent series resistance (ESR), which is a key parameter in influencing the charge/discharge rate, as a smaller ESR value represents a lesser internal loss and a greater charge/discharge rate.[52] The ESR value of KA-CNT/carbon-5 is only 0.15 Ω, but it gradually increases to 0.75 Ω for KA-CNT/carbon-50. The thicker the carbon shell, the longer the diffusion path and the lower the electron conductivity, as a result of higher ESR value.

To further illustrate the capacitance change of electrode materials with frequency and electrolyte ion transfer kinetics at different pore lengths, the real ($C'(\omega)$) and imaginary ($C''(\omega)$) capacitances versus frequency are plotted in Figure 11c,d, respectively. The evolution of $C'(\omega)$ normalized by $C'_{max}$ (1 mHz) versus frequency demonstrates a transition between purely resistive behavior ($C'(\omega)/C'_{max} = 0$) to purely capacitive behavior ($C'(\omega)/C'_{max} = 1$).[53] The capacitance of the KA-CNT/carbon core−shell nanocomposites shows saturation at a frequency below ∼0.1 Hz, suggesting that ion adsorption at near equilibrium could be achieved within seconds. Comparing the frequencies at which capacitance drops to 50% of its maximum value ($f_{0.5}$), we clearly see that the KA-CNT/carbon with a thinner microporous carbon shell demonstrates the faster frequency response (e.g., $f_{0.5}$ of 1.08 Hz for KA-CNT/carbon-5 and 0.07 Hz for KA-CNT/carbon-50). This result indicates that the ion diffusion at shorter pore length is more convenient. The faster ion diffusion should correlate with their better capacitance retention at higher current density in rate testing.

Figure 11d shows the evolution of the imaginary capacitance with frequency, demonstrating various peaks across the frequency spectrum. These capacitive peaks are related to the relaxation of the ion adsorbed in the pores and are related to the energy loss of the cell at the low-frequency range in the Nyquist plot.[54] A relaxation time constant ($\tau_0$) is the reciprocal of the frequency at the peak, which is the transition point of the cell from capacitive to resistive behavior and corresponds to the point of maximum energy dissipation. Thus, short relaxation time indicates fast frequency response of the supercapacitor. The $\tau_0$ values for KA-CNT/carbon-5, KA-CNT/carbon-10, KA-CNT/carbon-25, and KA-CNT/carbon-50 are 0.9, 1.6, 3.7, and 20.8 s, respectively, which are obviously related to the thickness of microporous carbon shell. These results give valuable insight into the role of pore length on the frequency response of microporous carbon materials.

## CONCLUSIONS

All-carbon-based CNT/microporous carbon core−shell nanocomposites, whose carbon shell thickness can be precisely controlled over the nanometer length scale, were produced by polymer surface coating of CNTs, followed by carbonization and controlled activation. The obtained nanocomposites have a unique core−shell nanostructure with a CNT as the core and high-surface-area microporous carbon as the shell. In such a unique hybrid structure, the CNTs offer multiple conducting channels to improve the electrical conductivity, improving the


DOI: 10.1021/am5087374
ACS Appl. Mater. Interfaces 2015, 7, 4817−4825

low electronic conductivity of microporous carbons. The 3D entangled network constructed by the CNTs affords easy and quick channels for mass (e.g., ion and electrolyte) transport. Short-pore-length microporous carbon shells with precisely tunable thickness could also minimize the ion paths within the microporous channels, boosting the power performance of the cell. The core−shell structure, benefiting from its rigidity, guarantees the long-term cycling stability of supercapacitors. Moreover, the proof-of-concept study of the correlation between composite structure and frequency response may provide some reference information for electrode material design and related applications.

## ■ ASSOCIATED CONTENT

### Supporting Information

SEM images, XRD patterns, TG curve, CV curves, and capacitance retention curves of the samples. This material is available free of charge via the Internet at http://pubs.acs.org.

## ■ AUTHOR INFORMATION

### Corresponding Author

*Tel: +86 21 64252924. Fax: +86 21 64252914. E-mail: longdh@mail.ecust.edu.cn.

### Notes

The authors declare no competing financial interest.

## ■ ACKNOWLEDGMENTS

This work was partly supported by MOST (2014CB239702) and National Science Foundation of China (Nos. 51302083, 51172071, and 51272077), and Fundamental Research Funds for the Central Universities and Shanghai Rising-Star Program.

## ■ REFERENCES

(1) Miller, J. R.; Simon, P. Electrochemical Capacitors for Energy Management. *Science* **2008**, *321*, 651−652.
(2) Winter, M.; Brodd, R. J. What Are Batteries, Fuel Cells, and Supercapacitors? *Chem. Rev.* **2004**, *104*, 4245−4270.
(3) Simon, P.; Gogotsi, Y. Materials for Electrochemical Capacitors. *Nat. Mater.* **2008**, *7*, 845−854.
(4) Xing, W.; Huang, C. C.; Zhuo, S. P.; Yuan, X.; Wang, G. Q.; Hulicova-Jurcakova, D.; Yan, Z. F.; Lu, G. Q. Hierarchical Porous Carbons with High Performance for Supercapacitor Electrodes. *Carbon* **2009**, *47*, 1715−1722.
(5) Zhang, L. L.; Zhao, X. S. Carbon-Based Materials as Supercapacitor Electrodes. *Chem. Soc. Rev.* **2009**, *38*, 2520−2531.
(6) Rose, M.; Korenblit, Y.; Kockrick, E.; Borchardt, L.; Oschatz, M.; Kaskel, S.; Yushin, G. Hierarchical Micro- and Mesoporous Carbide-Derived Carbon as a High-Performance Electrode Material in Supercapacitors. *Small* **2011**, *7*, 1108−1117.
(7) Xia, K.; Gao, Q.; Jiang, J.; Hu, J. Hierarchical Porous Carbons with Controlled Micropores and Mesopores for Supercapacitor Electrode Materials. *Carbon* **2008**, *46*, 1718−1726.
(8) Ou, Y. J.; Peng, C.; Lang, J. W.; Zhu, D. D.; Yan, X. B. Hierarchical Porous Activated Carbon Produced from Spinach Leaves as an Electrode Material for an Electric Double Layer Capacitor. *New Carbon Mater.* **2014**, *29*, 209−215.
(9) Yang, X.; Wu, D.; Chen, X.; Fu, R. Nitrogen-Enriched Nanocarbons with a 3-D Continuous Mesopore Structure from Polyacrylonitrile for Supercapacitor Application. *J. Phys. Chem. C* **2010**, *114*, 8581−8586.
(10) Pandolfo, A. G.; Hollenkamp, A. F. Carbon Properties and Their Role in Supercapacitors. *J. Power Sources* **2006**, *157*, 11−27.
(11) Snook, G. A.; Kao, P.; Best, A. S. Conducting-Polymer-Based Supercapacitor Devices and Electrodes. *J. Power Sources* **2011**, *196*, 1−12.
(12) Zhai, Y.; Dou, Y.; Zhao, D.; Fulvio, P. F.; Mayes, R. T.; Dai, S. Carbon Materials for Chemical Capacitive Energy Storage. *Adv. Mater.* **2011**, *23*, 4828−4850.
(13) Xu, B.; Wu, F.; Su, Y.; Cao, G.; Chen, S.; Zhou, Z.; Yang, Y. Competitive Effect of KOH Activation on the Electrochemical Performances of Carbon Nanotubes for EDLC: Balance between Porosity and Conductivity. *Electrochim. Acta* **2008**, *53*, 7730−7735.
(14) Li, Y.; Van Zijll, M.; Chiang, S.; Pan, N. KOH Modified Graphene Nanosheets for Supercapacitor Electrodes. *J. Power Sources* **2011**, *196*, 6003−6006.
(15) Qu, D.; S, H. Studies of Activated Carbons Used in Double-Layer Capacitors. *J. Power Sources* **1998**, *74*, 99−107.
(16) Huang, J.; Sumpter, B. G.; Meunier, V.; Yushin, G.; Portet, C.; Gogotsi, Y. Curvature Effects in Carbon Nanomaterials: Exohedral versus Endohedral Supercapacitors. *J. Mater. Res.* **2010**, *25*, 1525−1531.
(17) Largeot, C.; Portet, C.; Chmiola, J.; Taberna, P. L.; Gogotsi, Y.; Simon, P. Relation between the Ion Size and Pore Size for an Electric Double-Layer Capacitor. *J. Am. Chem. Soc.* **2008**, *130*, 2730−2731.
(18) Tung, V. C.; Chen, L. M.; Allen, M. J.; Wassei, J. K.; Nelson, K.; Kaner, R. B.; Yang, Y. Low-Temperature Solution Processing of Graphene−Carbon Nanotube Hybrid Materials for High-Performance Transparent Conductors. *Nano Lett.* **2009**, *9*, 1949−1955.
(19) Wang, D. W.; Li, F.; Liu, M.; Lu, G. Q.; Cheng, H. M. 3D Aperiodic Hierarchical Porous Graphitic Carbon Material for High-Rate Electrochemical Capacitive Energy Storage. *Angew. Chem.* **2008**, *47*, 373−376.
(20) Fan, Y.; Yang, X.; Zhu, B.; Liu, P. F.; Lu, H. T. Micro-mesoporous Carbon Spheres Derived from Carrageenan as Electrode Material for Supercapacitors. *J. Power Sources* **2014**, *268*, 584−590.
(21) Schnorr, J. M.; Swager, T. M. Emerging Applications of Carbon Nanotubes. *Chem. Mater.* **2011**, *23*, 646−657.
(22) Dumitrescu, I.; Unwin, P. R.; Macpherson, J. V. Electrochemistry at Carbon Nanotubes: Perspective and Issues. *Chem. Commun.* **2009**, *45*, 6886−6901.
(23) Chen, X.; Zhu, H.; Chen, Y. C.; Shang, Y.; Cao, A.; Hu, L.; Rubloff, G. W. MWCNT/$V_2O_5$ Core/Shell Sponge for High Areal Capacity and Power Density Li-Ion Cathodes. *ACS Nano* **2012**, *6*, 7948−7955.
(24) Zhang, B.; Liang, J.; Xu, C. L.; Wei, B. Q.; Ruan, D. B.; Wu, D. H. Electric Double-Layer Capacitors Using Carbon Nanotube Electrodes and Organic Electrolyte. *Mater. Lett.* **2001**, *51*, 539−542.
(25) Yang, L.; Shi, Z.; Yang, W. Polypyrrole Directly Bonded to Air-Plasma Activated Carbon Nanotube as Electrode Materials for High-Performance Supercapacitor. *Electrochim. Acta* **2015**, *153*, 76−82.
(26) Hughes, M.; Chen, G. Z.; Shaffer, M. S. P.; Fray, D. J.; Windle, A. H. Electrochemical Capacitance of a Nanoporous Composite of Carbon Nanotubes and Polypyrrole. *Chem. Mater.* **2002**, *14*, 1610−1613.
(27) Liu, M.; Miao, Y. E.; Zhang, C.; Tjiu, W. W.; Yang, Z.; Peng, H.; Liu, T. Hierarchical Composites of Polyaniline-Graphene Nanoribbons-Carbon Nanotubes as Electrode Materials in All-Solid-State Supercapacitors. *Nanoscale* **2013**, *5*, 7312−7320.
(28) Bi, R. R.; Wu, X. L.; Cao, F. F.; Jiang, L. Y.; Guo, Y. G.; Wan, L. J. Highly Dispersed $RuO_2$ Nanoparticles on Carbon Nanotubes: Facile Synthesis and Enhanced Supercapacitance Performance. *J. Phys. Chem. C* **2010**, *114*, 2448−2451.
(29) Hou, Y.; Cheng, Y.; Hobson, T.; Liu, J. Design and Synthesis of Hierarchical $MnO_2$ Nanospheres/Carbon Nanotubes/Conducting Polymer Ternary Composite for High Performance Electrochemical Electrodes. *Nano Lett.* **2010**, *10*, 2727−2733.
(30) Jiang, H.; Li, C.; Sun, T.; Ma, J. A Green and High Energy Density Asymmetric Supercapacitor Based on Ultrathin $MnO_2$ Nanostructures and Functional Mesoporous Carbon Nanotube Electrodes. *Nanoscale* **2012**, *4*, 807−812.
(31) Cai, F.; Kang, Y.; Chen, H.; Chen, M.; Li, Q. Hierarchical CNT@$NiCo_2O_4$ Core−Shell Hybrid Nanostructure for High-Performance Supercapacitors. *J. Mater. Chem. A* **2014**, *2*, 11509−11515.


DOI: 10.1021/am5087374
*ACS Appl. Mater. Interfaces* 2015, 7, 4817−4825

(32) Chuang, C. M.; Huang, C. W.; Teng, H.; Ting, J. M. Effects of Carbon Nanotube Grafting on the Performance of Electric Double Layer Capacitors. *Energy Fuels* **2010**, *24*, 6476−6482.
(33) Noked, M.; Okashy, S.; Zimrin, T.; Aurbach, D. Composite Carbon Nanotube/carbon Electrodes for Electrical Double-Layer Super Capacitors. *Angew. Chem.* **2012**, *51*, 1568−1571.
(34) Borenstien, A.; Noked, M.; Okashy, S.; Aurbach, D. Composite Carbon Nano-tubes (CNT)/Activated Carbon Electrodes for Non-aqueous Super Capacitors Using Organic Electrolyte Solutions. *J. Electrochem. Soc.* **2013**, *160*, A1282−A1285.
(35) Xu, G.; Ding, B.; Nie, P.; Shen, L.; Wang, J.; Zhang, X. Porous Nitrogen-Doped Carbon Nanotubes Derived from Tubular Polypyrrole for Energy-Storage Applications. *Chem.—Eur. J.* **2013**, *19*, 12306−12312.
(36) Fan, X.; Yu, C.; Ling, Z.; Yang, J.; Qiu, J. Hydrothermal Synthesis of Phosphate-Functionalized Carbon Nanotube-Containing Carbon Composites for Supercapacitors with Highly Stable Performance. *ACS Appl. Mater. Interfaces* **2013**, *5*, 2104−2110.
(37) Zhou, Y.; Qin, Z. Y.; Li, L.; Zhang, Y.; Wei, Y. L.; Wang, L. F.; Zhu, M. F. Polyaniline/Multi-walled Carbon Nanotube Composites with Core−Shell Structures as Supercapacitor Electrode Materials. *Electrochim. Acta* **2010**, *55*, 3904−3908.
(38) Frackowiak, E.; Khomenko, V.; Jurewicz, K.; Lota, K.; Beguin, F. Supercapacitors Based on Conducting Polymers/Nanotubes Composites. *J. Power Sources* **2006**, *153*, 413−418.
(39) Obreja, V. V. On the Performance of Supercapacitors with Electrodes Based on Carbon Nanotubes and Carbon Activated Material—A Review. *Physica E* **2008**, *40*, 2596−2605.
(40) Qian, X.; Lv, Y.; Li, W.; Xia, Y.; Zhao, D. Multiwall Carbon Nanotube@Mesoporous Carbon with Core−Shell Configuration: A Well-Designed Composite-Structure toward Electrochemical Capacitor Application. *J. Mater. Chem.* **2011**, *21*, 13025−13031.
(41) Teng, H.; Chang, Y. J.; Hsieh, C. T. Performance of Electric Double-Layer Capacitors Using Carbons Prepared from Phenol−Formaldehyde Resins by KOH Etching. *Carbon* **2001**, *39*, 1981−1987.
(42) Ahmadpour, A.; Do, D. D. The Preparation of Active Carbons from Coal by Chemical and Physical Activation. *Carbon* **1996**, *34*, 471−479.
(43) Teng, H.; Wang, S. C. Preparation of Porous Carbons from Phenol−Formaldehyde Resins with Chemical and Physical Activation. *Carbon* **2000**, *38*, 817−824.
(44) Walker, P. L., Jr. Production of Activated Carbons: Use of $CO_2$ versus $H_2O$ as Activating Agent. *Carbon* **1996**, *34*, 1297−1299.
(45) Chen, Y.; Liu, C.; Li, F.; Cheng, H. M. Pore Structures of Multi-walled Carbon Nanotubes Activated by Air, $CO_2$ and KOH. *J. Porous Mater.* **2006**, *13*, 141−146.
(46) Zhao, N.; He, C.; Jiang, Z.; Li, J.; Li, Y. Physical Activation and Characterization of Multi-walled Carbon Nanotubes Catalytically Synthesized from Methane. *Mater. Lett.* **2007**, *61*, 681−685.
(47) Tamai, Y.; Watanabe, H.; Tomita, A. Catalytic Gasification of Carbon with Steam, Carbon Dioxide and Hydrogen. *Carbon* **1977**, *15*, 103−106.
(48) Lillo-Rodenas, M. A.; Cazorla-Amoros, D.; Linares-Solano, A. Understanding Chemical Reactions between Carbons and NaOH and KOH: An Insight into the Chemical Activation Mechanism. *Carbon* **2003**, *41*, 267−275.
(49) Kierzek, K.; Frackowiak, E.; Lota, G.; Gryglewicz, G.; Machnikowski, J. Electrochemical Capacitors Based on Highly Porous Carbons Prepared by KOH Activation. *Electrochim. Acta* **2004**, *49*, 515−523.
(50) Inagaki, M.; Konno, H.; Tanaike, O. Carbon Materials for Electrochemical Capacitors. *J. Power Sources* **2010**, *195*, 7880−7903.
(51) Zhang, L. L.; Zhou, R.; Zhao, X. S. Graphene-Based Materials as Supercapacitor Electrodes. *J. Mater. Chem.* **2010**, *20*, 5983−5992.
(52) Portet, C.; Taberna, P. L.; Simon, P.; Flahaut, E. Influence of Carbon Nanotubes Addition on Carbon−Carbon Supercapacitor Performances in Organic Electrolyte. *J. Power Sources* **2005**, *139*, 371−378.
(53) Taberna, P. L.; Simon, P.; Fauvarque, J. F. Electrochemical Characteristics and Impedance Spectroscopy Studies of Carbon−Carbon Supercapacitors. *J. Electrochem. Soc.* **2003**, *150*, A292−A300.
(54) Garcia, B. B.; Feaver, A. M.; Zhang, Q.; Champion, R. D.; Cao, G.; Fister, T. T.; Nagle, K. P.; Seidler, G. T. Effect of Pore Morphology on the Electrochemical Properties of Electric Double Layer Carbon Cryogel Supercapacitors. *J. Appl. Phys.* **2008**, *104*, 014305.


DOI: 10.1021/am5087374
*ACS Appl. Mater. Interfaces* 2015, 7, 4817−4825